Journal of Power Sources 221 (2013) 406–418

Contents lists available at SciVerse ScienceDirect

Journal of Power Sources

journal homepage: www.elsevier.com/locate/jpowsour

Fuel cell Plug-in Hybrid Electric Vehicle anticipatory and real-time blended-mode energy management for battery life preservation

Sousso Kelouwani [a,*], Kodjo Agbossou [b], Yves Dubé [a], Loïc Boulon [b]

[a] Hydrogen Research Institute and the Department of Mechanical Engineering of Université du Québec à Trois-Rivières, 3351, boul. des ForgesC.P. 500, Trois-Rivières, Québec, G9A 5H7, Canada
[b] Hydrogen Research Institute and the Department of Electrical and Computer Engineering of Université du Québec à Trois-Rivières, Trois-Rivières, Québec, G9A 5H7, Canada

HIGHLIGHTS

- An anticipatory control method that reduces the battery discharges power during the vehicle acceleration phases.
- An optimal and real-time power splitting method that preserves the battery life and saves hydrogen fuel.
- A comparative study using three different driving cycles.

ARTICLE INFO

Article history:
Received 8 May 2012
Received in revised form
1 August 2012
Accepted 6 August 2012
Available online 23 August 2012

Keywords:
Electric vehicles
Energy efficiency
Energy management
Fuel cells
Nonlinear optimal control
Vehicle dynamics

ABSTRACT

In this paper, the energy management problem for a Fuel Cell Plug-in Hybrid Electric Vehicle is investigated using a real-time power splitting method that preserves the battery pack life. The reduction of high-power demand during the vehicle stop-and-go operations and the limitation of the batteries' minimum energy to a prescribed level are the two aspects considered in this study. Using a longitudinal motion model of an experimental small utility truck, a multi-criteria optimization problem, including the hydrogen/electricity cost ratio and the anticipation of the high-power demand, is formulated and solved. The analysis of the effects of the fuel cell and the battery efficiency degradations demonstrated that there exists a minimum cost ratio that prevents the Energy Management System to adequately limit the batteries' depletion with the contribution of the Fuel Cell power. The overall control system does not require a prior knowledge of the trip information. Therefore, the real-time implementation of this system is realistic. Compared with a rule-based Energy Management System, the proposed optimal and real-time approach provides up to 5% of hydrogen saving whilst maintaining the Battery Pack energy close to the minimum prescribed energy. The high-power demand reduction and the depletion limitation enable the Energy Management System to preserve the batteries' life.

1. Introduction

The use of fossil energy in the transportation sector is one of the greenhouse gas emission sources [1]. So, the vehicle powertrain electrification and hybridization have been identified as a way to reduce these pollutants and to increase the fuel usage efficiency [2]. Among the commonly found powertrain electrification approaches are the hybrid electric (HEV), the plug-in hybrid electric (PHEV) and the all range electric powertrains which are based solely on batteries (BEV) [2]. Nowadays, the lack of wide deployment of charging stations, combined with their limited operating range, make it difficult for the BEVs to achieve the same travel distance as the conventional gasoline vehicles. The PHEV with an internal-combustion engine can provide an extended range. However, the use of fossil energy contributes to the greenhouse gas emission [3,4].

Hydrogen has been identified as a clean energetic vector, and therefore, it can help to reduce greenhouse gas emissions when used for electrical propulsion [5]. Furthermore, on a strictly energetic point of view, the hydrogen specific energy (33.33 kWh kg^{-1}) is by greater than the best currently available battery specific energy (0.25 kWh kg^{-1}). Hydrogen can be used through a fuel cell or through a genset (engine-generator powered by hydrogen) [6].

The PHEV serial topology allows the range extender power source to charge the batteries [2]. Since this range extender power source is not required to track the vehicle power demand dynamics, it can be set to operate at it maximum efficiency. However, the

* Corresponding author. Tel.: +1 819 376 5011; fax: +1 819 376 5210.
E-mail addresses: sousso.kelouwani@uqtr.ca (S. Kelouwani), kodjo.agbossou@uqtr.ca (K. Agbossou), yves.dube@uqtr.ca (Y. Dubé), loic.boulon@uqtr.ca (L. Boulon).

0378-7753/$ – see front matter © 2012 Elsevier B.V. All rights reserved.
http://dx.doi.org/10.1016/j.jpowsour.2012.08.016

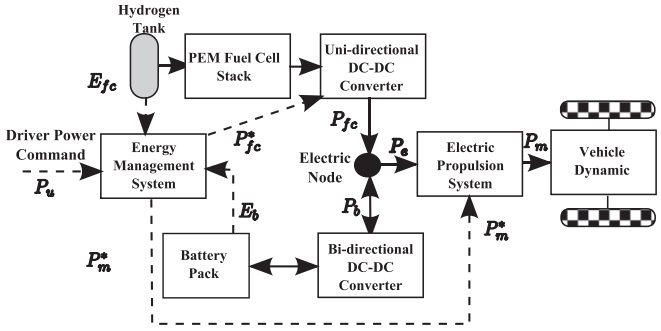

Fig. 1. Fuel cell hybrid electric vehicle: the arrows with the solid lines represent the energy flows; the arrows with the dashed lines represent the control and measured signals.

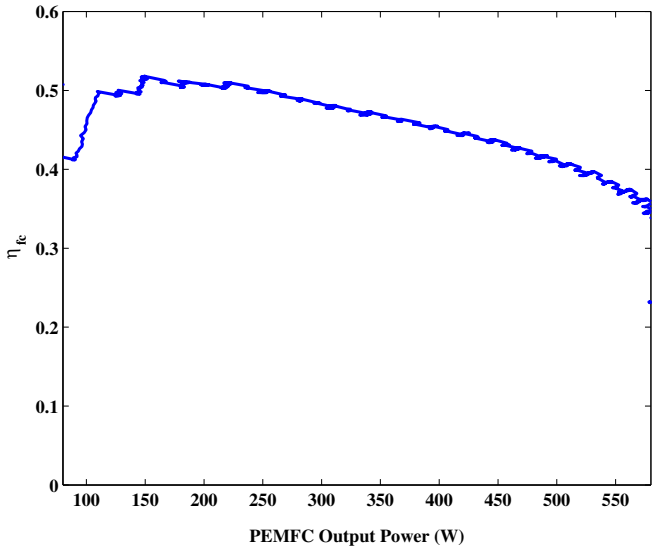

Fig. 2. Experimental Fuel Cell efficiency and power production.

battery power source and the electric traction system must be powerful enough to adequately track the vehicle user power demand [7,8].

In this paper, the energy management and the power splitting problems are thoroughly analyzed and a real-time optimal solution is proposed for a typical fuel cell and battery plug-in hybrid electric vehicle (FC-PHEV) with a serial topology. In addition, we focus mainly on the Proton Exchange Membrane Fuel Cell (PEMFC) because of: (i) the low operating temperature, (ii) the possibility for high current density and (iii) the good behavior under dynamic operating conditions [9].

It is well documented that the vehicle performance and the fuel savings are related to the power flow control between each energy source and the powertrain [10,11]. Among reported methods for the power flow control of FC-PHEV are the rule-based methods [12], the off-line optimal method and the near-optimal on-line method [13]. The rule-based methods use a set of predefined rules to split the power demand between the fuel cell and the batteries. These methods are simple, real-time, implementable and robust to traffic perturbation. Since they are mostly related to the Energy Management System designer, they cannot be widely used [2]. In addition, with rule-based methods, there is no formal way to assess the overall optimality. The off-line optimal methods aim at providing a more formal way to design the FC-PHEV energy management and power splitting systems [14]. However, their non-causal nature limits their use for real-time applications. The on-line optimal methods can be seen as the real-time version of the off-line methods. Usually, a local cost function is minimized with the in-line method whereas a global cost function is used to formulate the off-line solution. Some of the reported energy management methods have used the off-line solutions in order to adapt the in-line solution when the vehicle is moving [15,16].

In most of the reported works on the fuel cell vehicles, the fuel cell real behavior is not taken into account. Nevertheless, it is well documented that some fuel cell dynamics cannot adequately track the vehicle power demand [17,18]. Even if the PEMFC can sustain the power demand [19], the hybridization with a battery will improve the vehicle efficiency and will contribute positively to the fuel cell life span. A rapid power variation imposed on the fuel cell may result in the oxygen starvation [20]. On the other hands, the Battery Pack is sensitive to the ambient temperature and its life span is related to the depth of discharge, the number of charge/discharge cycles, the high-power discharge rate, etc [21].

This paper addresses the energy management and the power splitting problem with two main contributions. The first contribution is related to the analysis and the design of a real-time and efficient Energy Management System that incorporates the effect of the different sources' efficiency variation over the time. As the FC-PHEV is operating, various factors affect the power source efficiencies. In particular, we investigate the influence of the battery power source efficiency degradation on the power splitting method. The second contribution is related to the design of an optimal power splitting algorithm that preserves the battery life by limiting the depletion and by reducing the high-power discharges originating from the vehicle stop-and-go operations.

The rest of the paper is organized into six sections. The FC-PHEV control architecture and the vehicle model are presented in Section 2 and 3, respectively. Using this model, the energy management problem for the battery life preservation is formulated in Section 4 and solved in Section 5. The simulation results and the comparative study are discussed in Section 6, whereas the conclusion is presented in Section 7.

2. FC-PHEV serial control architecture

With the serial topology of a FC-PHEV as shown in Fig. 1, the fuel cell can operate at its maximum efficiency when recharging the batteries during the vehicle operation. We assume that the battery pack is adequately sized in order to meet the power demand during a trip. Fig. 2 shows an example of a real small scale PEMFC efficiency as a function of the power production. In this case, the maximum efficiency of 0.52 (see Equation (7)) is obtained with an output power of 150 W.

In Fig. 1, the uni-directional DC–DC converter is designated as the fuel cell power source, whereas the battery pack and the bi-directional DC–DC converter is considered as the battery power source. The power demand P_u from the vehicle driver is given to the Energy Management System (EMS) as a sequence of set points. Taking into account the available energy in the hydrogen tank E_{fc}, the available energy in the battery pack E_b and the different power source efficiencies, the EMS is responsible for finding the most appropriate power splitting of P_u. This power splitting process will lead to the generation of the power control signals P^*_{fc} (for the fuel cell power system) and P^*_m (for the Propulsion System). Given these power control signals, the uni-directional DC–DC converter will provide the corresponding electric power P_{fc} and the Propulsion System will deliver the corresponding P_m. P_b represents the battery power.

This architecture allows the battery power source to be fully responsible to track the driver power demand. At the same time,

the fuel cell operates at its maximum efficient in order to save hydrogen. Thus, the fuel cell power production management problem is to find the start and stop time sequence during the vehicle motion in order to minimize the hydrogen consumption and to keep the battery pack in a healthy state. In the paper, we assume that the battery healthy state is negatively affected by the depth-of-discharge (DOD) and by the high-power discharge rates: high DOD and high discharge rates will shorten the battery life span. Clearly, the role of the PEMFC in this architecture is to support the battery pack by:

- reducing the DOD;
- reducing the battery discharge rate;
- preventing the battery to be depleted below a minimum prescribed energy.

3. FC-PHEV longitudinal model for energy management

3.1. Energetic model

The longitudinal motion of the Fuel Cell PHEV is represented by Equation (1) [22] and the corresponding mechanical power is represented by (2).

$$F_v(k) = M_v\dot{v}(k) + \frac{1}{2}\rho_a C_d A_v v_d^2(k) + M_v g\sin(\theta(k)) + M_v g\mu\cos(\theta(k)) \quad (1)$$

where k, M_v, g, ρ_a, μ, C_d and A_v represent respectively the sampling index, the vehicle's total mass, the gravity constant, the air density, the rolling resistance coefficient, the air drag coefficient and the active frontal area; θ, $\dot{v}$ and v_d represent respectively the road grade, the longitudinal acceleration and the vehicle speed relative to the air. $0 < k < N$ where N is the number of samples in a given driving cycle.

$$P_m(k) = F_v(k)v(k) \quad (2)$$

The electric power P_e required for the vehicle propulsion depends mainly on the Electric Propulsion System efficiency η_m and P_m:

$$P_e(k) = \eta_m^{-1}(k)P_m(k) \quad (3)$$

The Equation (4) represents the power balance at the electric node (see Fig. 1). A positive value of the bi-directional converter power P_b represents the power from the Battery Pack whereas a negative value of P_b represents the power to the Battery Pack.

$$P_b(k) = \eta_m^{-1}(k)P_m(k) - P_{fc}(k) \quad (4)$$

The relationship between E_b and P_b is represented the following equation:

$$E_b(k+1) = E_b(k) - \eta_b^{-1}(k)P_b(k)\Delta T \quad (5)$$

where k, ΔT and η_b represent the sampling index, the sample time period and the battery power source efficiency (this efficiency includes the Bi-directional Converter and the Battery Pack efficiencies), respectively.

On an energetic point of view and assuming that the fuel cell parameters are adequately controlled, the following equation represents the energy balance in the Hydrogen Tank [20,23,24]:

$$E_{fc}(k+1) = E_{fc}(k) - K_{H2}\dot{m}_{H2}(k)\Delta T \quad (6)$$

where E_{fc}, K_{H2} and $\dot{m}_{H2}$ represent the hydrogen energy in the storage, the hydrogen high heating value [25,26] and the hydrogen flow rate, respectively. The fuel cell power system efficiency η_{fc} is defined as:

$$\eta_{fc}(k) = \frac{P_{fc}(k)}{K_{H2}\dot{m}_{H2}(k)} \quad (7)$$

One of the goals of the Fuel Cell is to reduce the impact of high Battery Pack discharge rate due to the propulsion system fast dynamics. These discharge periods are mostly related to the fast dynamics of the user power demand P_u, compared to the Fuel Cell dynamics. So the fuel cell power source dynamics need to be included into the Energy Management System. Equation (8) represents a first-order model of a PEMFC [20]:

$$P_{fc}(k+1) = A(k)P_{fc}(k) + B(k)P_{fc}^*(k) \quad (8)$$

where $0 \le A(k) \le 1$, $B(k)$ and $P_{fc}^*(k)$ represent respectively the Fuel Cell dynamic constant, the input coefficient and the input power command (see Fig. 1). The sequences of A and B can be determined through any classical system identification methods.

3.2. Fuel Cell and battery pack efficiency models

The Fuel Cell and the Battery Pack efficiency degradations are currently being investigated in the research community [27–30]. However, the reported results demonstrate that these phenomena are difficult to model precisely. So, to analyze the impact of the efficiencies on the overall management system, we use a semi-empirical approach based on the available power sources manufacture data.

3.2.1. Fuel Cell efficiency

The Fuel Cell degradation depends on several factors: number of voltage cycling, power level, power dynamics and ambient temperature and operating temperature. However, the detail interaction of these factors with the degration is complex. So we assume that for a constant power production, the Fuel Cell efficiency will decayed exponentially with the time [21,31] as represented by Equation (9). Even if the variable level of the FC power is used, a detailled relationship regarding the power level, the efficiency and the degradation can be used as well.

$$\eta_{fc}(k) = \eta_{fc}^0 e^{-D_{fc}k\Delta T} \quad (9)$$

where η_{fc}^0 and D_{fc} represent the fuel cell power source initial efficiency and the efficiency decay rate, respectively. ΔT is the sampling time.

We consider that the manufacturer provides the Fuel Cell lifetime t_{fc}. Knowing the Fuel cell initial efficiency (i.e. the measured efficiency when the Fuel Cell was used for the first time), D_{fc} is obtained using the following equation:

$$D_{fc} = -\frac{1}{t_{fc}}\ln\left(\frac{\eta_{fc}^e}{\eta_{fc}^0}\right)$$

where η_{fc}^e represents the minimum value corresponding to the Fuel Cell end-of-life efficiency.

3.2.2. Battery pack efficiency

The battery pack efficiency depends on several factors. The discharge power (or the discharge current) and the depth of discharge (DOD) are among the most influential parameters of the Battery Pack efficiency degradation [32,33]. Often, the manufacture provides two different maps [34]:

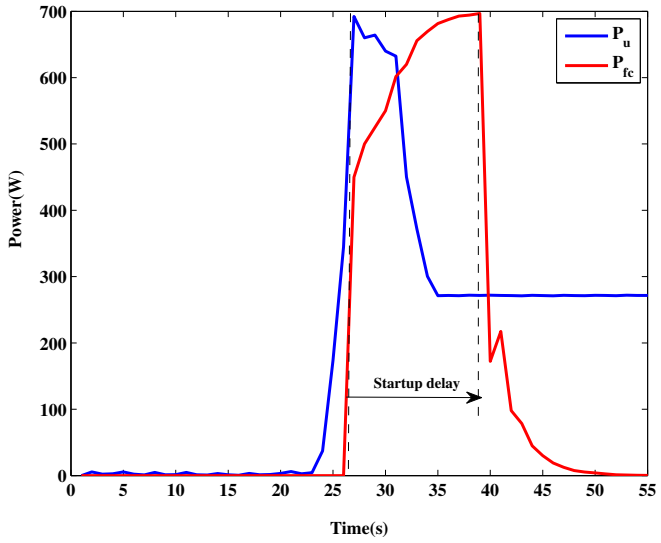

Fig. 3. Experimental Fuel Cell startup delay during a high discharge phase: P_u and P_{fc} represent the power demand and the fuel cell power, respectively.

- the battery capacity C_b as a function of the discharge current $I_b(k)$. Knowing the battery fully charge capacity $C_b(0)$, we defined the energetic efficiency map $\eta_b^e = F_1(C_b/C_b(0))$;
- the expected lifetime (or expected number of cycles) as a function of the DOD: $t_b^0 = F_2(\mathrm{DOD}(i))$; i represents the battery charge/discharge cycle index. The value of DOD(i) is updated at the end of the driving cycle i with the following equation and the battery is recharged completely for the next driving cycle:

$$\mathrm{DOD}(i) = \frac{\sum_{k=0}^{N} I_b(k)\Delta T}{C_b(0)}$$

N is the number of current samples for a given driving cycle i.

For each ΔT, the instantaneous efficiency $\eta_b^e(k)$ is retrieved using the map F_1. However, the value of $\eta_b^e(k)$ does not take into account the battery degradation effect represented by the map F_2. To include this effect, we define the degradation coefficient as follows:

$$\eta_b^d(k) = \frac{t_b(i-1)-1}{t_b^0}$$

where $t_b(i-1)$ is the remaining lifetime after the previous driving cycle. $0 \le \eta_b^d(k) \le 1, \forall k$.

The Battery Pack efficiency is obtained with the following equation:

$$\eta_b(k) = \eta_b^e(k)\eta_b^d(k) \tag{10}$$

Substituting $P_b(k)$ and $\eta_b(k)$ in Equation (5) with Equations (4) and (10), respectively, yields:

$$E_b(k+1) = E_b(k) - \left[\eta_b^e(k)\eta_b^d(k)\right]^{-1}\left[\eta_m^{-1}(k)P_m(k) - P_{fc}(k)\right]\Delta T \tag{11}$$

Taking into account the Fuel Cell efficiency, the hydrogen energy in the tank is always given by the following equation:

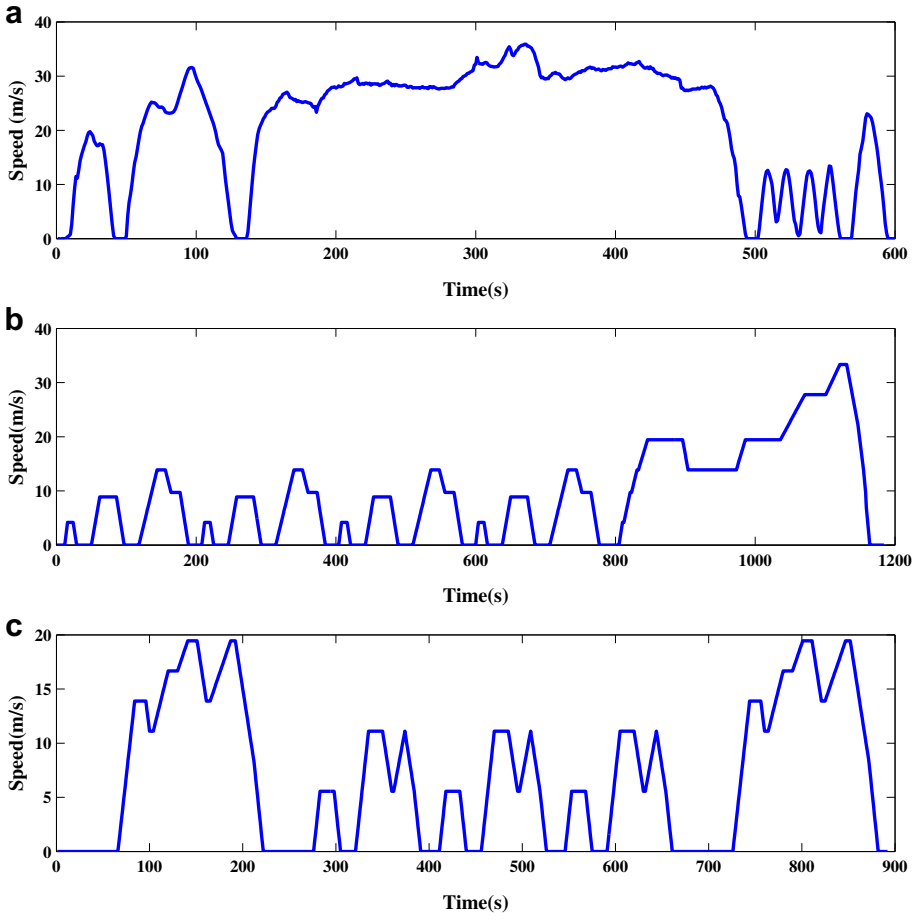

Fig. 4. Three different synthetic driving cycles: (a) US06 Driving Cycle, (b) New European Driving Cycle and (c) Japanese 10/15-Mode Driving Cycle.

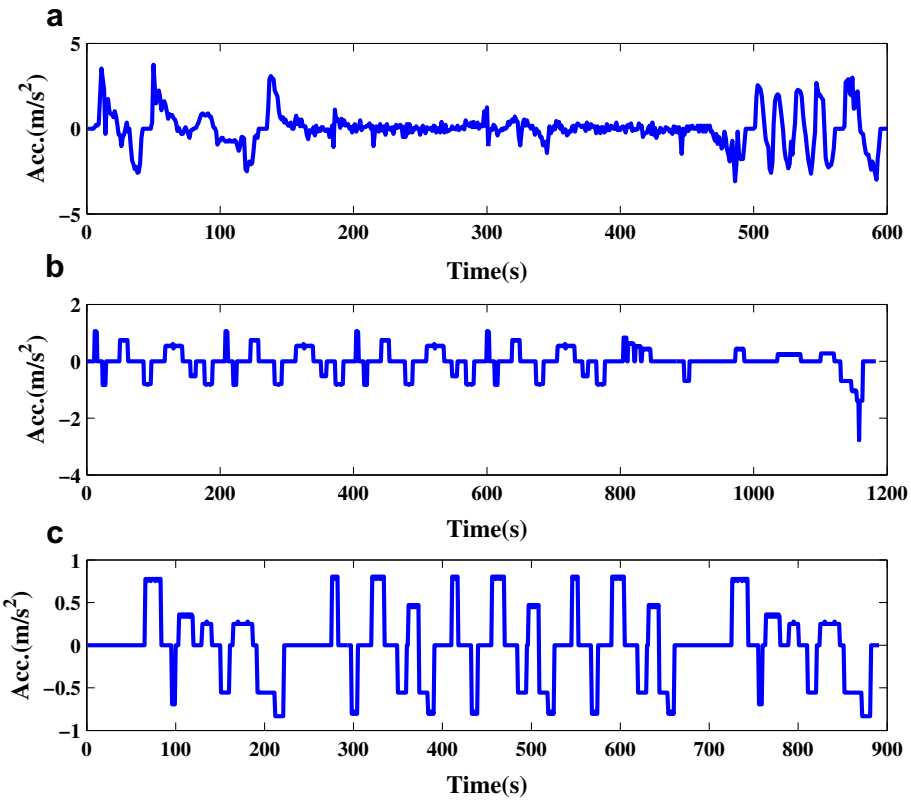

Fig. 5. Three acceleration profiles: (a) US06 Driving Cycle, (b) New European Driving Cycle and (c) Japanese 10/15-Mode Driving Cycle.

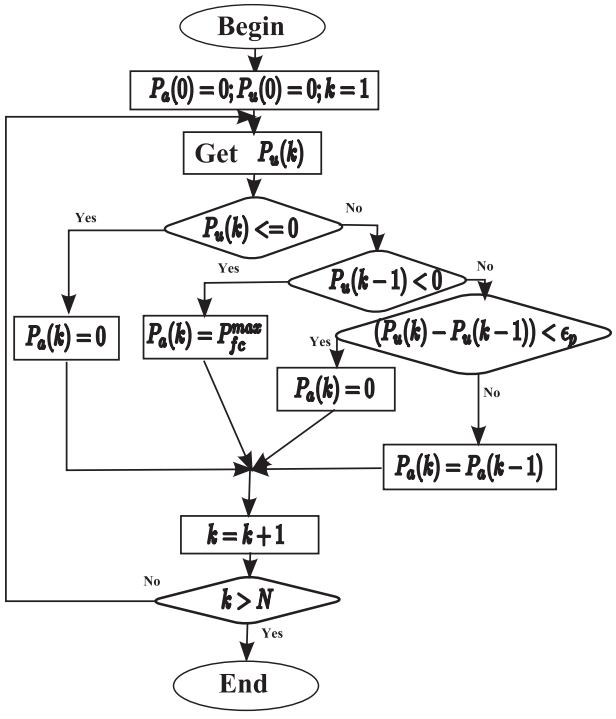

Fig. 6. High demand sequence generation: $\varepsilon_p < 0$ is a threshold indicating that P_u is decreasing sufficiently to assume that this high demand is ending.

$$E_{fc}(k+1) = E_{fc}(k) - \left[\eta_{fc}^{0} e^{-D_{fc} k \Delta T}\right]^{-1} P_{fc} \Delta T \tag{12}$$

Clearly, the hydrogen consumption and the Battery Pack energy consumption increase as the different power source efficiencies decrease over a long period of time. Since the amount of energy is limited, the following constraints must hold:

$$E_{fc}^{min} \leq E_{fc}(k) \leq E_{fc}^{max} \tag{13}$$

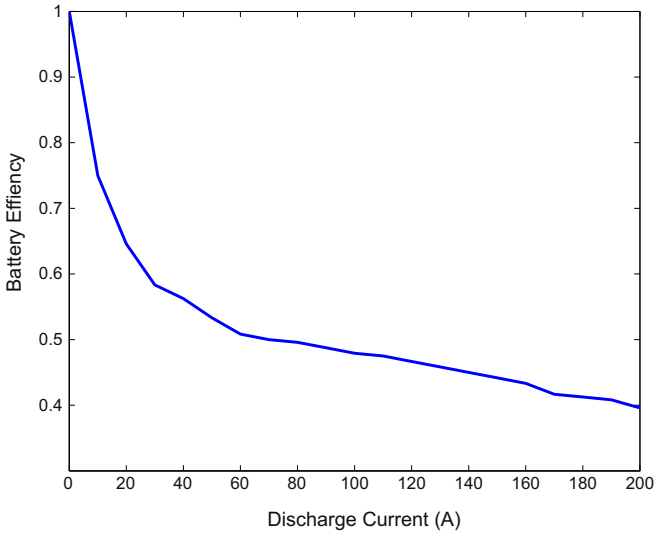

Fig. 7. A lead-acid battery efficiency curve [46].

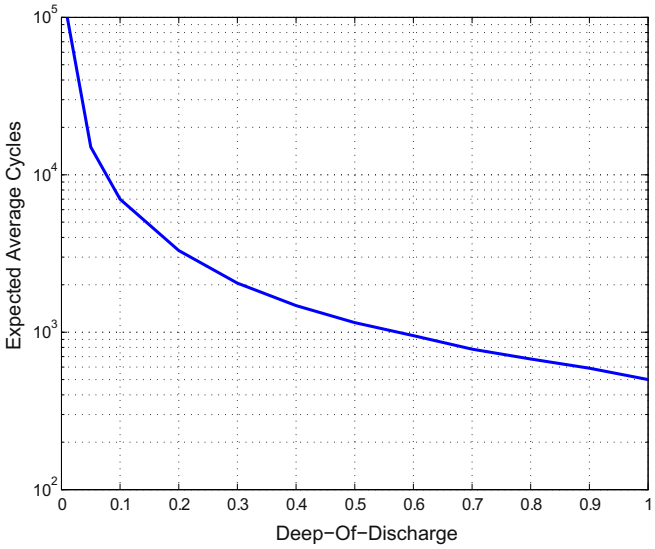

Fig. 8. Battery lifetime map [46].

$$E_b^{min} \le E_b(k) \le E_b^{max} \tag{14}$$

where $E_{fc}^{min}, E_{fc}^{max}, E_b^{min}$ and E_b^{max} represent the minimum hydrogen energy in the tank, the maximum hydrogen stored, the minimum Battery Pack energy and the maximum Battery Pack energy. E_b^{min} is defined as the minimum energy threshold that should be kept in the battery Pack in order to reduce its degradation. This value will play an important role for the Energy Management System.

4. Energy management problem formulation

4.1. High power discharge anticipation problem

One of the goals of the fuel cell power source is to reduce the impact of high discharge on the Battery Pack. The high discharge usually occurs during the vehicle acceleration phase. If the Fuel cell dynamics are similar (i.e. as quick as) to the vehicle dynamics, then it would be easier to start it at the beginning of these acceleration phases. Unfortunately, the slow Fuel Cell startup time imposes to anticipate the upcoming acceleration phases. Fig. 3 illustrates a typical high discharge during the vehicle acceleration. The fuel cell power reaches its maximum several second after the end of the high discharge phase. This example shows that the Fuel Cell should be started several seconds before this high discharge phase begins in order to reduce the negative impact on the Battery Pack.

4.2. Real-time power splitting problem

In motor mode, the Electric Propulsion System is supplied with the electric power P_e from the on-board power sources (Fuel Cell or Battery Pack: the arrows with the solid lines in Fig. 1). At each timestamp k, the human driver provides the desired power command $P_u(k)$. Given $P_u(k)$, the Energy Management System will generate the required optimal control signals for the fuel cell power source $P_{fc}^*(k)$ and for the Propulsion System $P_m^*(k)$. We propose in this section, a problem formulation that will allow a real-time generation of these optimal control signals in order to fulfill at least to the following conditions.

Table 1
PHEV parameters.

Parameter	Value	Parameter	Value
M_v	1200 kg	A_v	1.2 m^2
ρ_a	1.2 kgm^{-3}	μ	0.018
C_d	0.5		

Table 2
Simulation parameters.

Parameter	Value	Parameter	Value
$E_b(0)$	100 Wh	R_u	$100/3600^2$
η_m	0.9	R_{fc}	$10/3600^2$
E_b^{min}	50 Wh	C	1
E_b^{max}	100 Wh	E_{fc}^*	20 Ws
E_{fc}^{max}	100 Wh	η_{fc}^0	0.5
E_{fc}^{min}	0	D_{fc}	10^{-9}
P_{fc}^{max}	1500 W	ΔT	1 s
$A(k)$	0.72, $\forall k$	$B(k)$	0.95, $\forall k$

- The Battery Pack energy E_b should be kept above the safe energy threshold E_b^{min}. Complying with this condition will help to reduce Battery Pack degradation [35,36].
- The fuel cell power source should contribute to reduce the high power discharges from the Battery Pack. Complying with this condition will have two benefits: the improvement to the battery power source efficiency and the reduction of the Battery Pack degradation [37].
- The Fuel Cell must operate at its maximum efficiency in order to save hydrogen.

One way to simultaneously take into account the above mentioned conditions is to formulate an optimization problem with a multicriteria cost function. The proposed cost function (see Equation (15)) has two components. The first component $L(k)$ (Equation (16)) is the immediate cost whereas the second component φ (Equation (17)) represents the cost that will result in the application of the selected control signals $P_m^*(k)$ and $P_{fc}^*(k)$.

$$J(k) = L(k) + \phi \tag{15}$$

where:

$$L(k) = \frac{1}{2}\left(\left(E_b(k) - E_b^{min}\right)^2 + R_u(P_u(k) - P_m(k))^2 + R_{fc}\left(P_{fc}(k) - P_a(k)\right)^2 + C\dot{m}_{H2}^2\right) \tag{16}$$

Fig. 9. Experimental small utility truck FC-HEV.

and where:

$$\phi = \frac{1}{2}\left(E_b(k+1) - E_b^{min}\right)^2 \quad (17)$$

and where $R_u \geq 0$ is the penalty coefficient of the deviation between the driver power command and the actual power command sent to the propulsion system; $R_{fc} \geq 0$ is the penalty coefficient of the deviation between the fuel cell power and the anticipated power P_a based on the upcoming high discharge from the Battery Pack; C is the result of the division between the energy costs of hydrogen and electricity. We assume that the hydrogen energy is more expensive than the electricity energy. $C \geq 1$ is the hydrogen/electricity cost ratio applied to the hydrogen consumption $\dot{m}_{H2}$. According to Equations (7) and (9), the expression of $\dot{m}_{H2}$ is:

$$\dot{m}_{H2}(k) = \frac{P_{fc}(k)}{K_{H2}\eta_{fc}^0 e^{-D_{fc}k\Delta T}} \quad (18)$$

From Equation (16), the minimum of $L(k)$ is obtained when:

- the Battery Pack energy is close to the safe minimum value. This criterion will allow the Energy Management System to operate in charge depleting mode until E_b reaches E_b^{min}; in addition, since $C \geq 1$, the battery energy will be preferably used instead of the hydrogen energy
- the driver power demand P_u is close to the mechanical power P_m provided to the vehicle dynamics; this criterion will permit the vehicle to behave dynamically as desired by the driver;
- the hydrogen consumption rate is very low; this criterion will allow the use of the minimum hydrogen in order to fulfill to the other criteria;
- the fuel cell power P_{fc} is close to the anticipated high demand from the driver P_a; as said before, the dynamics of the Fuel Cell is slower than the power demand dynamics. So, it is necessary to anticipate the next upcoming high demand in order to allow enough time to the Fuel Cell to be powered up and contribute to the reduction of this high power discharge. A method for computing P_a is given in the next section.

The second component of $J(k)$ represented by φ (Equation (17)) is added in order to avoid depleting to much the Battery Pack, when the E_b becomes close to E_b^{min}.

Hence the optimization problem is formulated as follows: for each timestamp k, find the control signals $P_{fc}^*(k)$ and $P_m^*(k)$ so that the cost function (16) is minimized under the constraints represented by the following expressions:

1. $E_b(k+1) = E_b(k) - [\eta_b^0 e^{-D_b k\Delta T}]^{-1}[\eta_m^{-1}(k)P_m^*(k) - P_{fc}^*(k)]\Delta T$
2. $E_{fc}(k+1) = E_{fc}(k) - [\eta_{fc}^0 e^{-D_{fc}k\Delta T}]^{-1}P_{fc}^*\Delta T$
3. $P_{fc}(k+1) = A(k)P_{fc}(k) + B(k)P_{fc}^*(k)$
4. $E_{fc}^{min} \leq E_{fc}(k) \leq E_{fc}^{max}$
5. $E_b^{min} \leq E_b(k) \leq E_b^{max}$
6. In order to let the fuel cell to operate at its maximum efficiency, the value of P_{fc} must belong to $\{0, P_{fc}^{max}\}$ where P_{fc}^{max} represents the power produced with the maximum efficiency.
7. It is desirable to limit the number of the Fuel Cell start/stop cycles in order to reduce its degradation [38]. So the energy produced by the Fuel Cell during each start/stop cycle should be greater than a minimum value E_{fc}^* [30]. A large value of E_{fc}^* will let the Fuel Cell to work during a long period. As a result, the number of start/stop cycles will be smaller than if the E_{fc}^* is small.

In the next section, we propose a new method to solve this optimization problem.

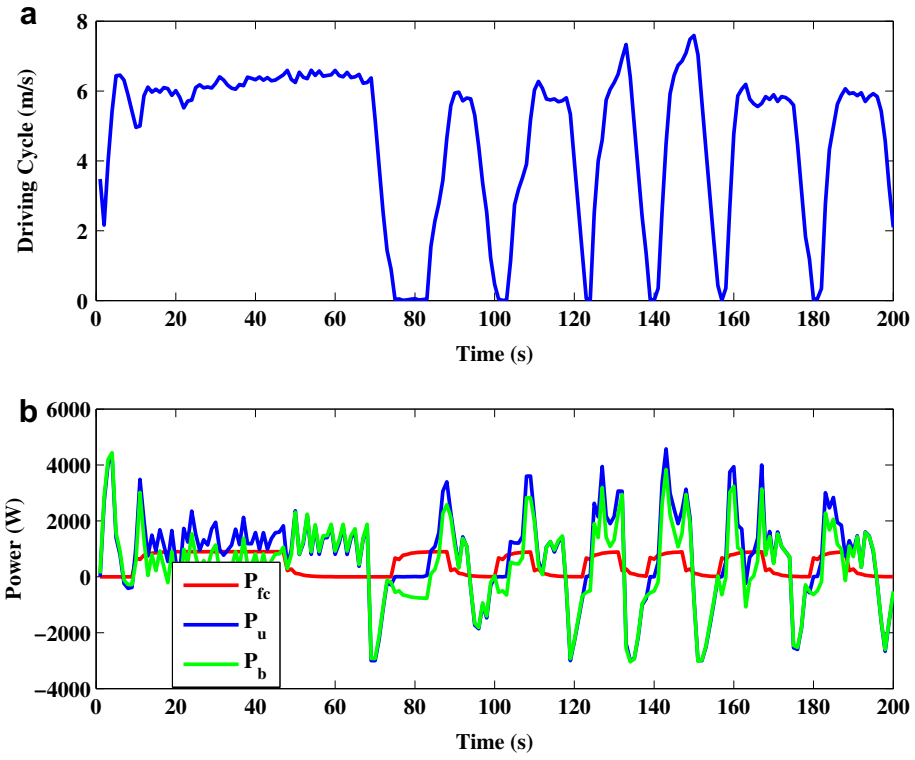

Fig. 10. Fuel Cell power production based on the high-power demand anticipation: (a) driving cycle with six stops-and-go, (b) power demand P_u, Fuel Cell power P_{fc} and battery pack power P_b.

5. Optimal power splitting solution

5.1. High power discharge anticipation algorithm

The first step for solving the aforementioned optimization problem is to determine the sequence of anticipated high power discharge $P_a(k)$, $k = 1,2,3,\ldots$ One way to find P_a is to train a neural network in order to predict the next occurrence of high power discharge. However, the convergence rate may be very slow. Thus, we propose a simple and efficient method to find P_a.

The high power discharge from Battery Pack is mainly due to the vehicle acceleration imposed by the driver. Often, this acceleration happens in two situations. The first one is related to the vehicle motion transition from a deceleration phase to an acceleration phase. In this case, the vehicle is doing a stop-and-go or a slow-down-and-go. The second situation occurs when the vehicle accelerates from a steady speed. In practice, the first situation occurs most of the time. So, it is possible to anticipate the upcoming acceleration by observing when the deceleration occurred.

Fig. 4 shows three commonly used synthetic driving cycles: the high acceleration aggressive driving schedule of the United States Environmental Protection Agency (US06) [39,40], the New European Driving Cycle (NEDC) [41] and the Japanese 10/15 Mode Driving Cycle (J1015) [42]. The acceleration profiles obtained from these driving cycles are shown in Fig. 5 and suggest that most of the time, a deceleration phase is followed by an acceleration phase until the cycles are completed.

Hence, Fig. 6 represents the algorithm used to generate the anticipate high power discharge signal P_a based upon the knowledge about the driver power demand P_u. We consider that a deceleration phase happens when $P_u \leq 0$. It is important to mention that the algorithm is not trying to predict when the driver will stop. Instead, it observes the deceleration phase and uses this knowledge to trigger the fuel cell operation. One can start the Fuel Cell at the beginning of a deceleration phase (when $P_u < 0$). However, the positive value of the Fuel Cell power could limit the ability of the battery to properly handle the regenerative power that may be produced during the vehicle deceleration. To avoid this drawback, we propose to start the Fuel Cell at the end of the deceleration phase which is represented by the transition between a negative value of P_u and the following positive value of P_u. In operation, the stack must be set to produce the power at its maximum efficiency P_{fc}^{max}. The Fuel Cell is stopped at the end of the acceleration phase.

The anticipatory algorithm assumes that if the difference between the current high-power demand value and the previous one is less than a given threshold $\varepsilon_p < 0$ when $P_u > 0$, then the high demand is decreasing. So, the Fuel Cell can be stopped. One possible way to determine $\varepsilon_p < 0$ is to consider the average power demand and use the following equation:

$$\varepsilon_0 = -\frac{\sum_{j=0}^{k} P_u(j)}{k},\ k>0 \tag{19}$$

The proposed algorithm is real-time because no a prior knowledge of the entire driving cycle is required and all involve processing are simple algebraic operations. Given the sequence of $P_u(k)$, $k = 1, 2,\ldots, N$, the optimal solution of the splitting problem is presented in the next section.

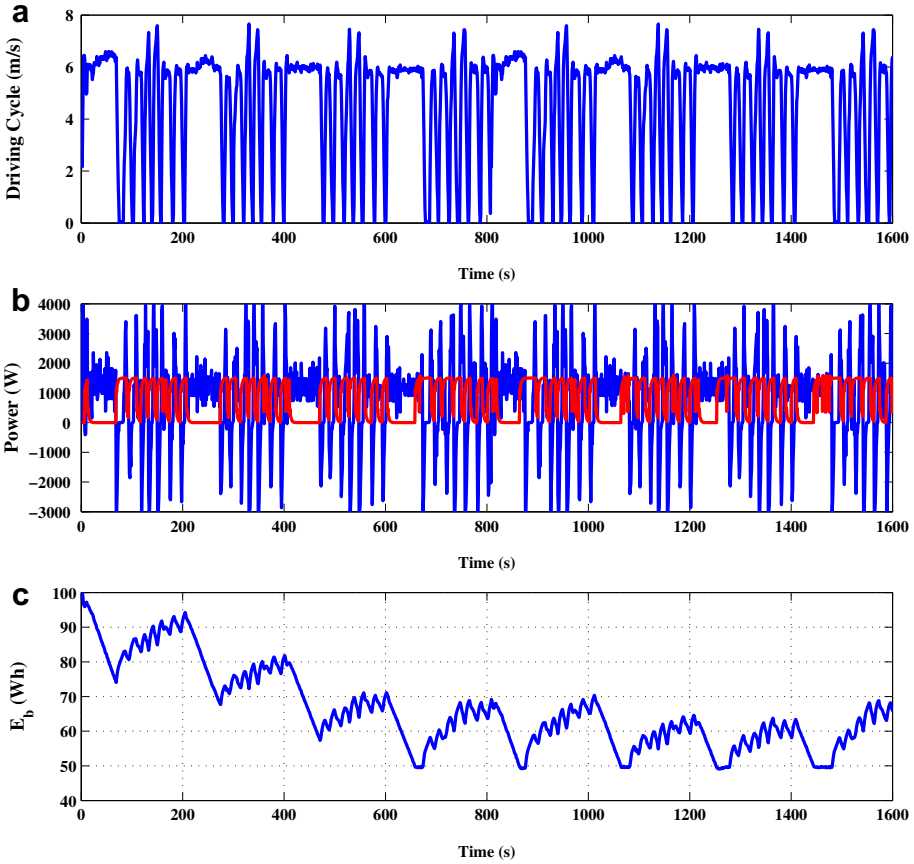

Fig. 11. Simulation with high efficiencies for the battery pack and the Fuel Cell: (a) driving cycle; (b) power demand P_u, Fuel Cell power P_{fc} and battery pack power P_b; (c) battery pack energy profile.

5.2. Locally optimal power splitting solution

Several methods exist to solve this static and nonlinear optimization problem [43]: iterative descent methods, approximation methods and dual and primal-dual methods. We have used the line search algorithm for nonlinear programming as outlined in Ref. [43]. This algorithm is selected because it provides an iterative optimization method that is simple and efficient to handle for real-time applications.

Line search method: The generic algorithm of line search is an iterative method which involves two main steps [44]:

- the search of a descent direction along the cost function $J(k)$;
- the selection of a step size along the selected direction.

In this paper, we used an enhanced line search algorithm originally proposed in Ref. [45]. Γ delimits the control signal search domain on which the optimization is performed. This domain is divided is ($N_{fc} \times N_m$) control signal grid points where N_{fc} and N_m represent the number of equal intervals on the P_{fc} dimension and on the P_m dimension, respectively. Using each grid point as an initial guess, the line search algorithm described in Ref. [45] is used in order to find local minimums. The optimal control signals P_{fc}^* and P_m^* are control signals P_{fc} and P_m that produce the smallest value of $J(k)$ by considering all minimums found using the grid points as the initial guesses and by considering all constraints involved in the problem formulation.

The controller obtained uses 2000 grid points ($N_{fc} = 2$, $N_m = 1000$). This number of points allows a real-time search of the optimums P_{fc}^* and P_m^*. For all performed simulation, the maximum execution time of the line search method is 0.98 ms on a Personal Computer (PC) with Pentium IV 3 GHz.

6. Simulation and discussion

The simulation pursues three main objectives: (i) the validation of the Fuel Cell power production through the anticipative algorithm; (ii) the analysis of the impact of the power system efficiency deteriorations on the overall real-time Energy Management System proposed in this paper; (iii) the comparative study of the energy saving between the proposed method and a typical rule-based energy management method [2].

6.1. Simulation context

The vehicle and the simulation parameters are summarized in Table 1 and Table 2, respectively. These vehicle parameters correspond to the small utility truck shown in Fig. 9 and which is being used in our research. We used a scale down factor of 0.01 on the power request and the different energy storage in order to match the fuel cell rated power of Fig. 9. The vehicle has an on-board Fuel Cell system (with a rated power of 1500 W) to recharge the Battery Pack. A 72 V lead-acid battery pack is used as the electric energy storage. For the simulation, we considered that the FC response delay is 5 s. At the beginning of each simulation, we assume that the Battery Pack is fully charged and no a prior knowledge of the driving cycle is available. The efficiency map and the lifetime map are represented in Figs. 7 and 8, respectively [46,47]. The system must rely only on the current and the past data collected. The Fuel Cell system is also assumed to be properly controlled by a PID controller.

6.2. Fuel Cell anticipative power production validation

To validate the Fuel Cell power production with the proposed anticipative algorithm, we consider the driving cycle represented in

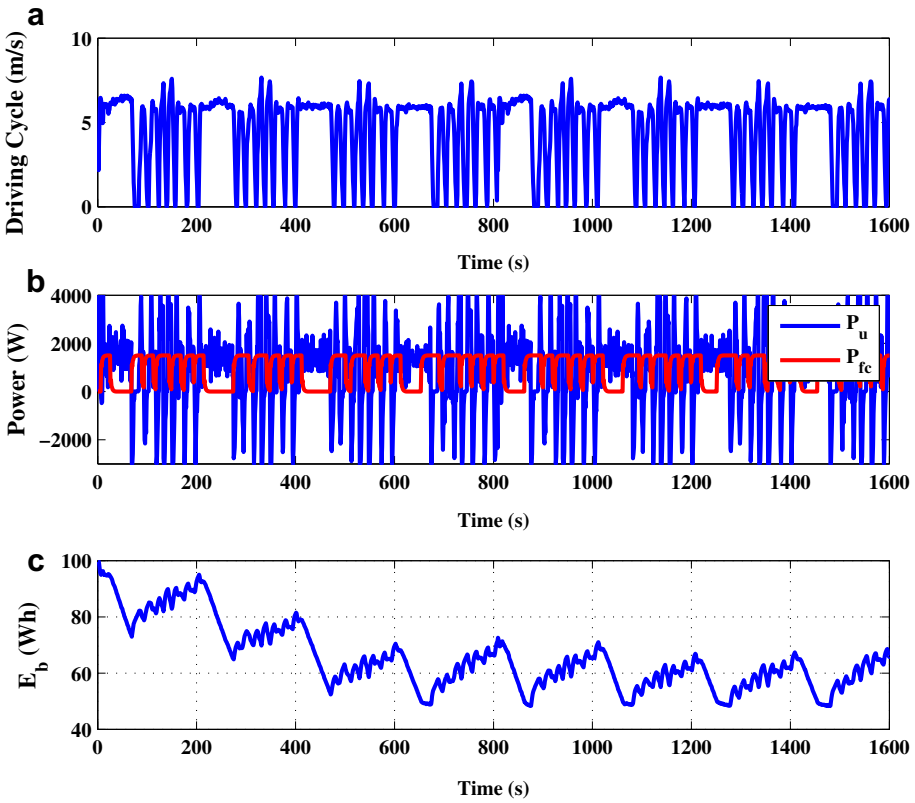

Fig. 12. Simulation with low efficiencies for the battery pack and the Fuel Cell: (a) driving cycle; (b) power demand P_u, Fuel Cell power P_{fc} and battery pack power P_b; (c) Battery pack energy profile.

Fig. 10 (graph (a)) and which is obtained with the vehicle shown in Fig. 9. This driving cycle has six stops-and-go, which reflect a typical usage of such a utility truck. The blue curve (in web version) in the graph (b) (Fig. 10) represents the power demand P_u. Except for the starting high-power demand (timestamp $k = 0$), where the Fuel Cell was not powered on, we observe in the graph (b) of Fig. 10 that the anticipative algorithm can track each subsequent high-power demand from the driver. Furthermore, the Fuel cell starts at the end of each deceleration phase and stops as soon as the corresponding high-power demand is ending. As a result, the peak power drawn from the Battery Pack is reduced by 29.5% in average (see the green curve (in web version) in the graph (b)). In addition, the Fuel Cell power production does not interfere with the regenerative power (the negative part of P_b coincides with the negative part of P_u). Due to its slow dynamics, if two stops-and-go are too close to each other, the Fuel Cell will be powered on at the beginning of the first one and will be stopped at the end of the deceleration phase of the second one. This fuel cell control behavior is observed during the time interval between 155 s and 168 s (see the graph (b), Fig. 10).

6.3. Impact of the hydrogen/electricity cost ratio and the power source efficiency deterioration

Two important parameters influence the energy management system and the power splitting algorithm: the power source efficiencies and the hydrogen/electricity cost ratio. To analyze the impact of the battery power system efficiency η_b, we used the driving cycle presented in Fig. 10 (in the graph (a)). We conducted two different simulations in order to demonstrate the effectiveness of the proposed energy management and power splitting methods:

- in the first simulation, we assume that the Battery Pack is new. Thus, the efficiency η_b is high;
- in the second simulation, the Battery Pack degradation is high and the efficiency is low.

During simulation, η_{fc} is assumed to change slowly (see parameters in Table 2).

6.3.1. Battery power system with high efficiency

Fig. 11 shows the Fuel Cell power generation when the two efficiencies are high. We see in the graph (c) of this figure that the Battery Pack energy is most of the time greater or close to the minimum energy to keep in the batteries ($E_b^{min} = 50$ Wh). In addition, the Fuel Cell can compensate for the high-power demand due to the stop-and-go as shown in the graph (b) of Fig. 11.

The cost function (15) has two conflicting requirements: (i) maintain the battery energy greater than E_b^{min} by using the fuel cell energy; (ii) minimize the hydrogen energy cost which is represented ($C \times \dot{m}_{H2}^2$). Note that $C \geq 1$ is set by the user as an input parameter. When the hydrogen/electricity cost ratio C increases, the Energy Management System reduces the use of hydrogen by decrease the Fuel Cell power production in order to minimize the cost function represented by Equation (15). Hence, the Battery Pack is depleted in order to meet the power demand. There exist a cost

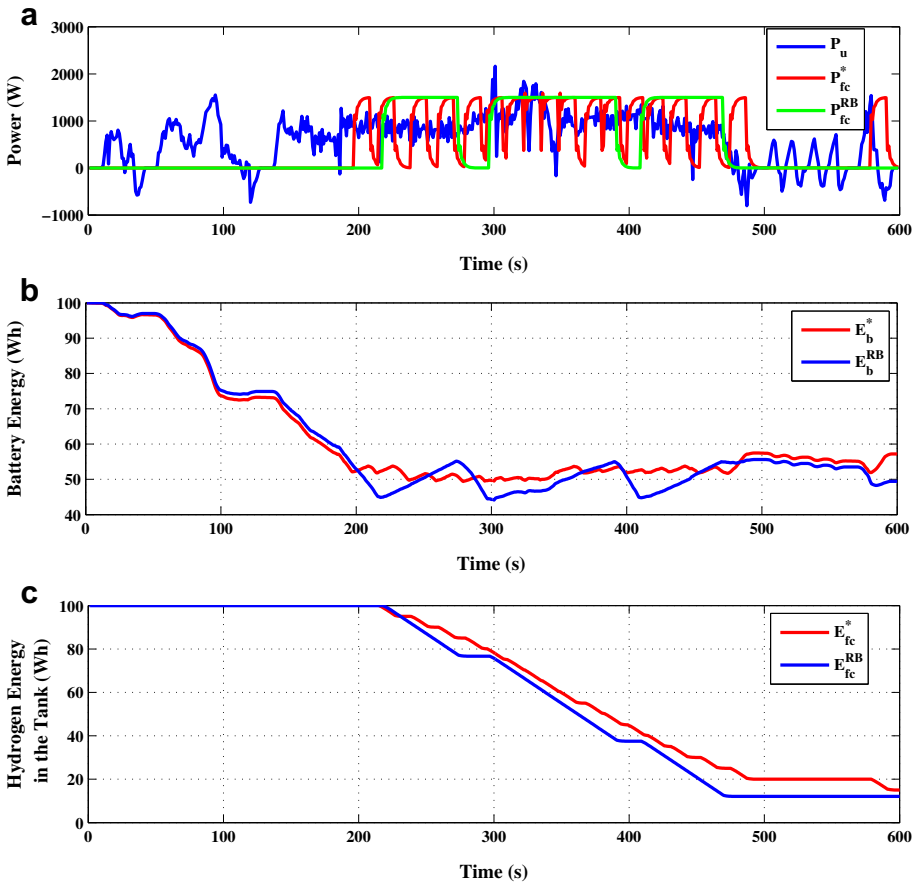

Fig. 13. Comparative study with US06 Driving Cycle: (a) power demand P_u, Fuel Cell optimal power production P_{fc}^* and Fuel Cell power production with the rule-based method P_{fc}^{RB}; (b) battery pack optimal energy profile E_b^* and battery pack rule-based energy profile E_b^{RB}; (c) stored hydrogen with the optimal energy profile E_{fc}^* and stored hydrogen with the rule-based energy profile E_{fc}^{RB}

value for which the Fuel Cell contribution cannot help to maintain the Battery Pack final energy $E_b(N)$ close to E_e^{min}. We designated this specific cost value as the critical cost. By increasing the cost ratio from 1 to 100, we found that this critical cost ratio is 10 for the power system with high efficiencies. Thus, if the cost ratio is lower than 10, the Energy Management System can maintain the healthy level of the Battery Pack using the Fuel Cell power production.

6.3.2. Battery power system with low efficiency

When the battery is aging, it efficiency decreases. So more hydrogen is needed to maintain its minimum energy above E_b^{min} during the driving cycle and the Energy Management System must adapt its power splitting algorithm accordingly. Fig. 12 shows a typical result with a low efficiency for the battery. The operating time between a start and a stop of the Fuel Cell is longer when the Battery Pack efficiency is low compared to the previous case for which the efficiency is high (see the graph (b) in Fig. 12 and the graph (b) in Fig. 11). In addition, the battery energy is kept greater or close to E_b^{min} during the driving cycle.

To analyze the effect of the hydrogen/electricity cost ratio on the capacity to maintain the battery depletion close to E_b^{min}, we run several simulations with different values of C. These results indicate that the value of the stored hydrogen at the end of the driving cycle $E_{fc}(N)$ are lower than their corresponding values obtained when the battery efficiency is high. Indeed, as the battery power source is less efficient than the Fuel Cell, more hydrogen is used to produce the propulsion energy. Thus, the Energy Management System can reduce the use of the less efficient power source in favor of the most efficient one. Since the Battery Pack energy is reduced in the low efficiency case, the cost ratio corresponding to the critical point ($C = 36$) is much greater than the cost ratio corresponding to the critical point obtained when the efficiency is high.

6.4. Comparative study

We consider the high efficiency for the Battery Pack and three commonly used driving cycles (see Fig. 4). The aim of the comparative study is to show the effectiveness of the proposed Energy Management System by analyzing the E_b and E_{fc} dynamics when one of the three driving cycles is used. For comparative purposes, a commonly used rule-based method for real-time energy management is considered. This method lets the Fuel Cell to start and to stop if E_b is lower than a predefined lower limit and if E_b is higher than a predefined high limit, respectively. For the comparative tests, the upper limit of E_b is set to $E_b^{up} = 55$ Wh and lower limit is set to $E_b^{down} = 45$ Wh. E_b^{min} is set to 50 Wh. Since the Fuel Cell maximum power is limited to 1500 W and the average power demand using the different driving cycles is much greater, we introduced a scale down factor of 0.01.

Figs. 13–15 show the comparative study results. The hydrogen energy used for the three driving cycles (graph (c) of Figs. 13–15) when the optimization method proposed in this paper used is less than the ones obtained with the rule-based method. Furthermore, for the three driving cycles, the E_b at the end of the cycles is always greater or close to E_b^{min} when the optimization method is used. These results demonstrate that the proposed method is efficient in preventing the Battery Pack to be over depleted.

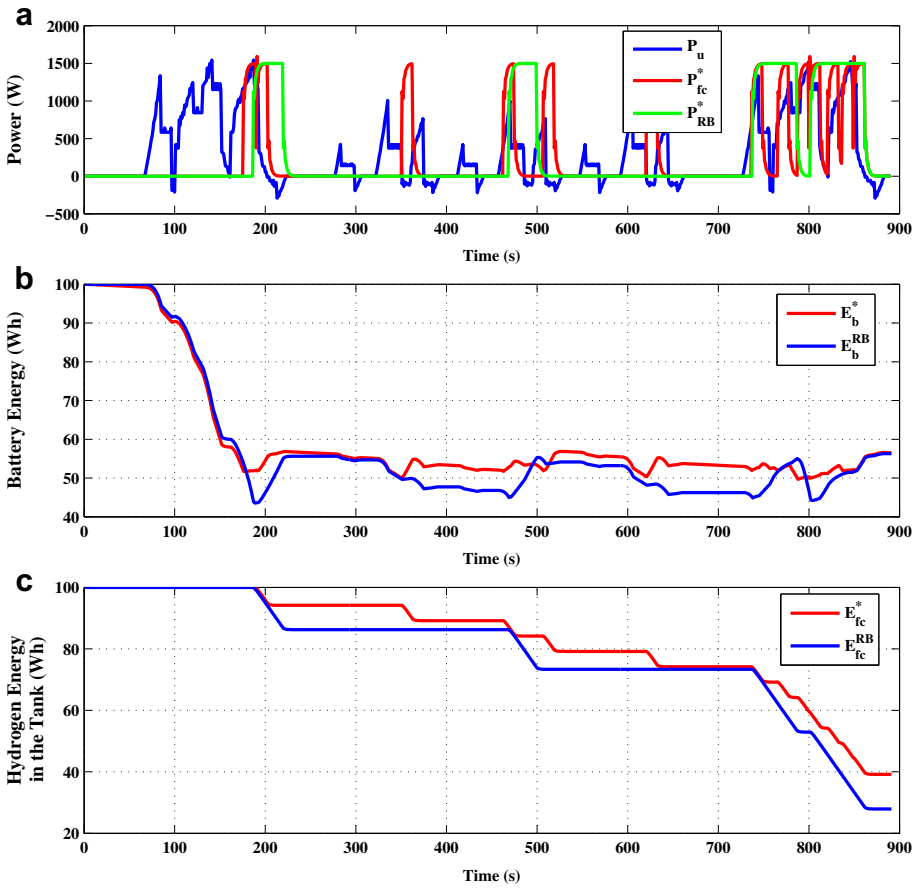

Fig. 14. Comparative study with NEDC Driving Cycle: (a) power demand P_u, Fuel Cell optimal power production P_{fc}^* and Fuel Cell power production with the rule-based method P_{fc}^{RB}; (b) battery pack optimal energy profile E_b^* and battery pack rule-based energy profile E_b^{RB}; (c) Stored hydrogen with the optimal energy profile E_{fc}^* and stored hydrogen with the rule-based energy profile E_{fc}^{RB}

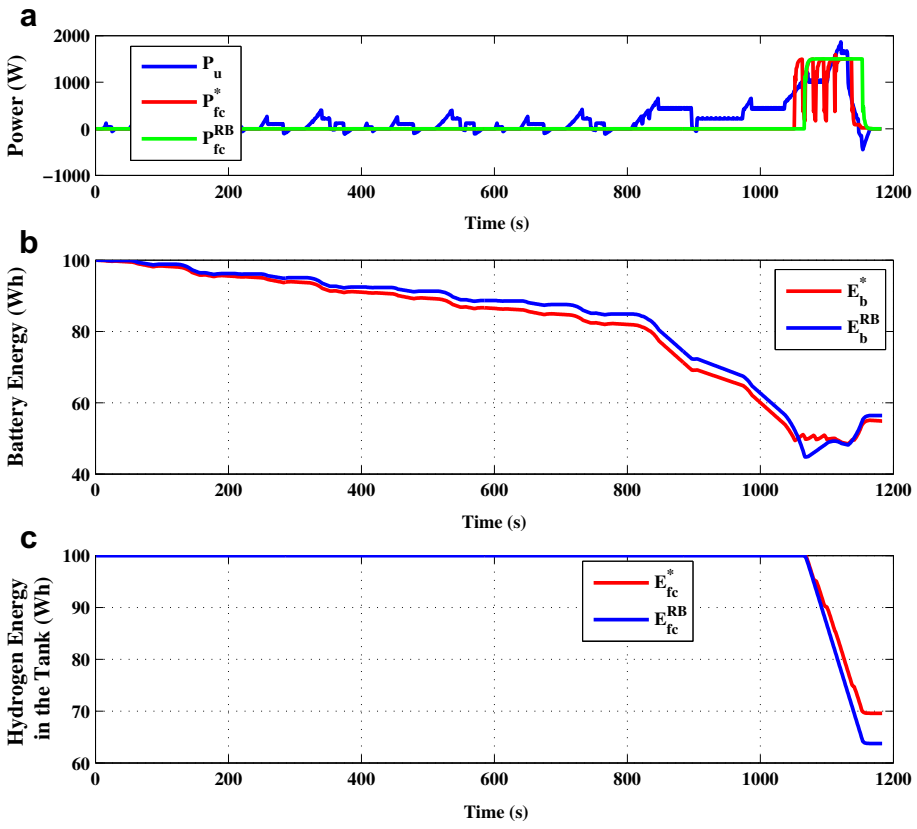

Fig. 15. Comparative study with J10/15 Driving Cycle: (a) power demand P_u, Fuel Cell optimal power production P^*_{fc} and Fuel Cell power production with the rule-based method P^{RB}_{fc}; (b) battery pack optimal energy profile E^*_b and battery pack rule-based energy profile E^{RB}_E; (c) stored hydrogen with the optimal energy profile E^*_{fc} and stored hydrogen with the rule-based energy profile E^{RB}_{fc}

Table 3
Degradation analysis results.

Efficiency	US06		NEDC		J10/15	
	Optimized	Rule-based	Optimized	Rule-based	Optimized	Rule-based
η^d_b after 100 h	98.6%	98.0%	99.3%	99.0%	97.0%	98.3%
η^d_b after 200 h	96.7%	95.7%	98.4%	97.4%	96.5%	94.4%

To analyze the effect of the Battery Pack degradation η^d_b on the proposed energy management system, we ran three simulations using the extended versions of the three driving cycles (US06, NEDC, J10/15). Each extended driving cycle is obtained by concatenating the original driving cycle in order to obtain a total of 5000 h. Using the battery efficiency curve (Fig. 7) and the battery lifetime map (Fig. 8), we investigate the degradation when the rule-based algorithm or the optimal method is used. We considered that when the DOD is greater than 75%, the Battery Pack is completely recharged and the hydrogen tank if fully filled. The following table summarizes the results.

In Table 3, η^d_e values when the optimized method is used is greater than the corresponding values when the rule-based method is used. These results suggest that the optimal energy management system is more effective to preserve the Battery Pack lifetime than the rule-based method.

7. Conclusion

A strategy for a Fuel Cell-PHEV based on optimal power splitting between the Battery Pack and the Fuel Cell is proposed and discussed. This power splitting method aims at: (i) reducing the high-power demand on the batteries, especially during the vehicle stop-and-go operations and (ii) preventing the excessive depletion which may shorter the Battery Pack life span. An experimental small utility truck longitudinal model was built and used for the control design and analysis. To reduce high-power demand, the Energy Management System uses an anticipatory control technique. Furthermore, a multi-criteria optimization including the hydrogen/electricity cost ratio and the anticipatory control is formulated and solve using the line search method. The overall control system does not require a prior knowledge of the trip information. Therefore, the real-time implementation of this Energy Management System is realistic. The analysis of the effects of the efficiency degradations on the system demonstrated that there exist a cost ratio value which prevents the Energy Management System to adequately limit the batteries depletion with the contribution of the Fuel Cell power.

Three commonly found driving cycles was used to validate and perform the comparative study. Compared with a rule-based Energy Management System, the optimal and real-time method proposed in this paper provide up to 5% of hydrogen saving whilst

maintaining the Battery Pack energy close to the minimum prescribed energy. The high-power demand reduction and the depletion limitation enable the Energy Management System to preserve the batteries life.

Acknowledgment

This work was supported by “Bureau de l’efficacité et de l’innovation énergétiques, Ministère des Ressources naturelles et de la Faune du Québec” and Natural Science and Engineering Research Council of Canada.

References

[1] P. Poudenx, Transportation Research Part A: Policy and Practice 42 (2008) 901–909.
[2] S. Wirasingha, A. Emadi, Vehicular Technology, IEEE Transactions on 60 (2011) 111–122.
[3] Z. Amjadi, S. Williamson, in: Electrical Power Energy Conference (EPEC), IEEE, 2009, pp. 1–7.
[4] C. Norman, N. Kaushal, C. Hendrickson, S. Peterson, J. Whitacre, J. Michalek, Journal of Mechanical Design, Transactions of the ASME 132 (2010) 1–11.
[5] D. Feroldi, M. Serra, J. Riera, Vehicular Technology, IEEE Transactions 58 (2009) 4720–4729.
[6] R. Moore, K. Hauer, D. Friedman, J. Cunningham, P. Badrinarayanan, S. Ramaswamy, A. Eggert, Journal of Power Sources 141 (2005) 272–285.
[7] A. Wang, W. Yang, in: Intelligent Control and Automation, 2006, WCICA 2006, The Sixth World Congress on, vol. 2, pp. 8324–8328.
[8] G. Paganelli, S. Delprat, T. Guerra, J. Rimaux, J. Santin, in: Vehicular Technology Conference, 2002, VTC Spring 2002, IEEE 55th, vol. 4, pp. 2076–2081.
[9] A. Stefanopoulou, K.-W. Suh, Control Engineering Practice 15 (2007/03) 277–289.
[10] A. Sciarretta, L. Guzzella, Control Systems, IEEE 27 (2007) 60–70.
[11] G. Wang, P. Yang, J. Zhang, in: Intelligent Control and Information Processing (ICICIP), 2010 International Conference, pp. 555–560.
[12] X. Li, J. Li, L. Xu, M. Ouyang. VPPC ’09, in: Vehicle Power and Propulsion Conference, IEEE, 2009, pp. 1749–1754.
[13] Z. Yu, D. Zinger, A. Bose, Journal of Power Sources 196 (2011/02/15) 2351–2359.
[14] J. Kessels, M. Koot, P. van den Bosch, D. Kok, Vehicular Technology, IEEE Transactions 57 (2008) 3428–3440.
[15] P. Pisu, G. Rizzoni, Control Systems Technology, IEEE Transactions 15 (2007) 506–518.
[16] N. Kim, S. Cha, H. Peng, Control Systems Technology, IEEE Transactions 19 (2011) 1279–1287.
[17] F. Gao, B. Blunier, M. Simoes, A. Miraoui, A. El-Moudni, IEEE Transaction on Energy Conversion 26 (2011) 184–194.
[18] G. Bucci, F. Ciancetta, E. Fiorucci, E. Rotondale, F. Veglio, International Symposium on Power Electronics, Electrical Drives, Automation and Motion (IEEE Cat. No. 06EX1320C) (2006). pp. 20–10.
[19] R. Moore, K. Hauer, G. Randolf, M. Virji, Journal of Power Sources 162 (2006) 302–308.
[20] A. Arce, A.J. Del Real, C. Bordons, D.R. Ramirez, IEEE Transactions on Industrial Electronics 57 (2010) 1892–1905.
[21] R. Gemmen, C. Johnson, Journal of Power Sources 159 (2006) 646–655.
[22] S. Kermani, R. Trigui, S. Delprat, B. Jeanneret, T. Guerra, Vehicular Technology, IEEE Transactions 60 (2011) 782–792.
[23] R. Methekar, S. Patwardhan, R. Gudi, V. Prasad, Journal of Process Control 20 (2010/01) 73–82.
[24] N. Bizon, Applied Energy 87 (2010) 3115–3130.
[25] A. del Real, A. Arce, C. Bordons, Journal of Power Sources 173 (2007/11/08) 310–324.
[26] K. Adegnon, Y. Dube, K. Agbossou, 2009 Canadian Conference on Electrical and Computer Engineering (CCECE 2009) (2009) 716–19.
[27] R. Silva, T. Hashimoto, G. Thompson, C. Rangel, International Journal of Hydrogen Energy (2012).
[28] S. Mu, P. Zhao, C. Xu, Y. Gao, M. Pan, International Journal of Hydrogen Energy 35 (2010) 8155–8160.
[29] P.A. Garca-Salaberri, M. Vera, R. Zaera, International Journal of Hydrogen Energy 36 (2011) 11856–11870.
[30] J. Wu, X.Z. Yuan, J.J. Martin, H. Wang, J. Zhang, J. Shen, S. Wu, W. Merida, Journal of Power Sources 184 (2008) 104–119.
[31] S. Zhang, X. Yuan, H. Wang, W. Mrida, H. Zhu, J. Shen, S. Wu, J. Zhang, International Journal of Hydrogen Energy 34 (2009) 388–404.
[32] M. Kellaway, P. Jennings, D. Stone, E. Crowe, A. Cooper, Journal of Power Sources 116 (2003) 110–117.
[33] J. Vetter, P. Novk, M. Wagner, C. Veit, K.-C. Mller, J. Besenhard, M. Winter, M. Wohlfahrt-Mehrens, C. Vogler, A. Hammouche, Journal of Power Sources 147 (2005) 269–281.
[34] H. Bindner, T. Cronin, P. Lundsager, J.F. Manwell, U. Abdulwahid, I. Baring-gould, Riso National Laboratory 1515 (2005) 1–81.
[35] C.-S.N. Shiau, N. Kaushal, C.T. Hendrickson, S.B. Peterson, J.F. Whitacre, J.J. Michalek, Journal of Mechanical Design, Transactions of the ASME 132 (2010) 091013.
[36] F. Martel, Y. Dube, L. Boulon, L. Agbossou, in: Vehicle Power and Propulsion Conference (VPPC), 2011 IEEE International Conference, pp. 1–8.
[37] J. Stevens, G. Corey, in: Photovoltaic Specialists Conference (1996). Conference Record of the Twenty Fifth IEEE, pp. 1485–1488.
[38] W. Schmittinger, A. Vahidi, Journal of Power Sources 180 (2008) 1–14.
[39] Q. Gong, Y. Li, Z.-R. Peng, Vehicular Technology, IEEE Transactions 57 (2008) 3393–3401.
[40] S. Moura, H. Fathy, D. Callaway, J. Stein, Control Systems Technology, IEEE Transactions 19 (2011) 545–555.
[41] M. Koot, J. Kessels, B. de Jager, W. Heemels, P. van den Bosch, M. Steinbuch, Vehicular Technology, IEEE Transactions 54 (2005) 771–782.
[42] A. Sciarretta, M. Back, L. Guzzella, Control Systems Technology, IEEE Transactions 12 (2004) 352–363.
[43] D. Bertsekas, Nonlinear Programming, Optimization and Neural Computation Series, Athena Scientific (1995).
[44] N.I.M. Gould, S. Leyffer, An Introduction to Algorithms for Nonlinear Optimization (2003).
[45] C. Grosan, A. Abraham, Modified Line Search Method for Global Optimization (2007).
[46] USBattery, Expected Cycle Life vs. DOD. Available from: (2012) http://www.usbattery.com/usb_images/cycle_life.xls.pdf.
[47] USBattery, Product Capacity Chart. Available from: (2012) http://www.usbattery.com/usb_images/USB%20Capacity%20Chart.pdf.